Electron density compression and oscillating effects on laser energy absorption in overdense plasma targets

Z. Y. Ge,[1] H. B. Zhuo,[1,*] W. Yu,[2] X. H. Yang,[1] T. P. Yu,[1] X. H. Li,[1] D. B. Zou,[1] Y. Y. Ma,[1] Y. Yin,[1] F. Q. Shao,[1] and X. J. Peng[3]

[1]*College of Science, National University of Defense Technology, Changsha 410073, P. R. China*

[2]*Shanghai Institute of Optics and Fine Mechanics, Chinese Academy of Sciences, Shanghai 201800, P. R. China*

[3]*Institute of Applied Physics and Computational Mathematics, Beijing 100088, P. R. China*

(Received 27 October 2013; revised manuscript received 22 January 2014; published 25 March 2014)

An analytical model for energy absorption during the interaction of an ultrashort, ultraintense laser with an overdense plasma is proposed. Both the compression effect of the electron density profile and the oscillation of the electron plasma surface are self-consistently included, which exhibit significant influences on the laser energy absorption. Based on our model, the general scaling law of the compression effect depending on laser strength and initial density is derived, and the temporal variation of the laser absorption due to the boundary oscillating effect is presented. It is found that due to the oscillation of the electron plasma surface, the laser absorption rate will vibrate periodically at ω or 2ω frequency for the p-polarized and s-polarized laser, respectively. The effect of plasma collision on the laser absorption has also been investigated, which shows a considerable rise in absorption with increasing electron-ion collision frequency for both polarizations.

DOI: 10.1103/PhysRevE.89.033106 PACS number(s): 52.38.Dx, 52.25.Os, 52.50.Jm

I. INTRODUCTION

The interaction of intense laser pulse with highly overdense plasmas offers very promising applications such as coherent and incoherent x-ray production [1,2], high harmonic generation [3], plasma-based particle acceleration [4–7], and high-energy electron production [8,9]. Knowing how much laser energy can be converted to thermal or directed kinetic energy of charged plasma particles is of critical importance to these applications. Early work in the context of inertial confinement fusion focused on the inverse bremsstrahlung in underdense, coronal plasma profiles due to the low laser intensities at that time [10]. With the advent of short-pulse, high-intensity lasers in the early 1990s, new mechanisms have been postulated to explain the high absorption measured experimentally in regimes where the collisional absorption became ineffective, such as resonance absorption [11], $J \times B$ heating [12], vacuum heating [13–15], etc. To understand the basic physics of laser–overdense-plasma interaction and obtain quantitative predictions, some approximation must be made, also the detail electron dynamics should be simplified. For example, a recent model developed by Haines *et al.* [16] predicts increasing absorption with higher intensity, albeit with a highly simplified assumption for the hot electron flux and restricted to normally incident light. Good agreements with experimental results in the high-intensity regime are shown in an analytical model presented by Gibbon *et al.* [17], in spite that the electron dynamics is also simplified and the results are based on the choice of a special attenuation factor of the pump strength.

Recently ultrashort (sub-10 fs) laser pulses with a high contrast ratio (10^{10}) and relativistic intensity ($>10^{18}$ W/cm^2) have been realized by using either plasma mirrors or parametric amplifications [18,19]. It allows the laser field to directly interact with solid matter, where the plasma is highly overdense and collisional. On the other hand, the light pressure of the ultraintense laser pulse will exceed the thermal pressure and compress the electrons to an equilibrium position where the induced electrostatic field can balance the light pressure [20]. Furthermore, under the driving of the 2ω ponderomotive force or the longitudinal component of the laser electric field, the electron plasma surface will oscillate periodically [21]. To our knowledge, there is no proper theoretical model to understand the details of the ultrashort laser absorption, including the novel electron density compression and oscillating effects. So, a generally applicable, quantitative theory which can describe the influences of the electron density compression and oscillating effects on laser absorption is still lacking.

In this article an analytical model describing this scenario is presented. Within the assumption of cold-fluid approximation, this one-dimensional (1D) model captures the quantitative aspects of the laser energy absorption. Combined with the oscillation of the electron plasma surface, it also manages to reproduce the salient features of laser absorption from the electron wall piled up by the light pressure. In particular, we clarify the influence of the electron density compression effect and the oscillation of the electron plasma surface on laser absorption. For small laser intensities or high plasma densities, the compression effect and the oscillation of the electron plasma surface are nearly turned off, which however, shows a considerable higher absorption. Electrons are accelerated toward the target by the oscillating laser field and then gain energy from the evanescent wave. For higher laser intensities or lower plasma densities, subjected to the light pressure, the electrons are pushed into the target, forming an electron-depleted layer where the 2ω ponderomotive force or the longitudinal component of the laser electric field will drive the electron plasma surface to oscillate. Due to the high-density electron wall, the incident laser will be reflected more thoroughly, resulting in a significant decrease of the laser absorption.

This paper is structured as follows. In Sec. II the cold-fluid model describing this scenario is presented and the compression effect of the electron density is illustrated. Section III deals with the compression and oscillating effects on s-polarized

*Corresponding author: hongbin.zhuo@gmail.com

laser absorption, whereas the solution for p-polarized laser absorption is studied in Sec. IV. Finally, we compare the theoretical results with experimental data and discuss our model in Sec. V.

II. COLD-FLUID MODEL AND COMPRESSION OF ELECTRON DENSITY

We consider an ultrashort, strong laser pulse irradiating on a solid-density target at an angle θ from the z direction. The half space $z \geqslant 0$ is assumed to be initially filled by a neutral, homogeneous plasma of electron density $n_e = N_0$. On the time scale ($t < 10$ fs), the plasma density is not affected by the usual hydrodynamic plasma expansion, and is highly overdense and collisional [22]. The ion motion during the process of interest is negligible and can be ignored. Furthermore, the quiver velocity of the electron in the laser field is much higher than the electron thermal velocity, so that the plasma can be assumed to be cold. Our starting point is the Lorentz equation of motion for the electrons in a cold, unmagnetized plasma, plus the Maxwell equations:

$$\partial_t \mathbf{p} = -e\mathbf{E} - m_e c^2 \nabla\gamma, \tag{1}$$

$$\nabla \times \mathbf{E} = -(1/c)\partial_t \mathbf{B}, \tag{2}$$

$$\nabla \cdot \mathbf{E} = 4\pi e(Zn_i - n_e), \tag{3}$$

$$\nabla \times \mathbf{B} = (1/c)\partial_t \mathbf{E} - (4\pi/c)en_e\mathbf{u}, \tag{4}$$

where $\mathbf{p} = \gamma m_e \mathbf{u}$, $\mathbf{u}$ and $\gamma = \sqrt{1 + p^2/m_e^2c^2}$ are the electron velocity and relativistic factor. n_e, n_i, m_e, c, and Z mean the electron density, ion density, electron mass, the light speed, and the ion charge number, respectively. Electromagnetic fields, space, density, and time coordinates are normalized as $(\mathbf{E},\mathbf{B}) \to (\mathbf{E},\mathbf{B})e/m_e\omega c$, $(x,y) \to (x,y)k$, $n_e \to n_e/n_c$, and $t \to \omega t$. Here $n_c = m_e\omega^2/4\pi e^2$ is the critical density, ω and k denote the laser frequency and wave number, respectively.

When the laser pulse impinges on the plasma surface, electrons are quickly pushed inward by the light pressure. The electrons pile up, leaving behind a charge depletion layer and giving rise to an electrostatic field back-holding them. We assume that the electrons quickly reach an equilibrium position where the electrostatic field balances the light pressure exactly. Thus, a density jump is formed at the position of the effective vacuum-plasma interface z_b. Below the density jump ($z < z_b$), electrons are totally pushed out (i.e., $n_e = 0$). While beyond the density jump, the electron density can be compressed to a very high level in a narrow region [23]. For the profile of the electron density $n_e(z)$ in $z \geqslant z_b$, in the intense laser intensity ($a_L \gg 1$) and highly overdense plasma ($n_e \gg n_c$) limits, a quantitative estimate is feasible by [24]

$$n_e(z) = \delta n_b e^{(z_b - z)/l_s} + N_0, \tag{5}$$

where $\delta n_b = Ne_b - N_0$, and Ne_b is the peak value of the electron density piled up at z_b. For the skin depth l_s we expect $l_s \approx \lambda_b = \sqrt{n_c/Ne_b}\,\lambda$ [25], with λ being the wavelength of the laser pulse. The balance between the total radiation pressure and the electrostatic force reads

$$E_0(z_b)e \int_{z_b}^{+\infty} [n_e(z) - n_i(z)]dz/2 \approx 2I\cos\theta/c, \tag{6}$$

where $E_0(z_b)$ is the electrostatic field at z_b. From Poisson equation (3) we obtain

$$E_0(z_b) = 4\pi e \int_{-\infty}^{z_b} n_i(z)dz. \tag{7}$$

Conservation of the total electric charge requires

$$\int_{z_b}^{+\infty} [n_e(z) - n_i(z)]dz = \int_{-\infty}^{z_b} n_i(z)dz. \tag{8}$$

From Eqs. (6)–(8) the explicit expressions of z_b and Ne_b can be described by

$$z_b = \left(\frac{1}{\sqrt{2}}\frac{a_L/\pi}{N_0/n_c}\sqrt{\cos\theta}\right)\lambda, \tag{9}$$

$$Ne_b = N_0 + \frac{\alpha^2 N_0^2}{2n_c} + \frac{\alpha N_0}{\sqrt{n_c}}\sqrt{N_0 + \frac{\alpha^2 N_0^2}{4n_c}}, \tag{10}$$

respectively, with $a_L = eE/m_e\omega c$ (the normalized laser amplitude), and $\alpha = z_b/\lambda$. To obtain this expression we have taken $I\lambda^2 = \pi P_0 a_L^2/2 = [1.37\times10^{18}\ \mathrm{W\,cm^{-2}\,\mu m^2}]a_L^2$, with $P_0 = m_e^2c^5/e^2 = 8.67$ GW [26]. Thus the general scaling law of the electron density compression effect is derived.

Of particular interest is the dependence of the compression effect upon the laser strength a_L and the initial plasma density

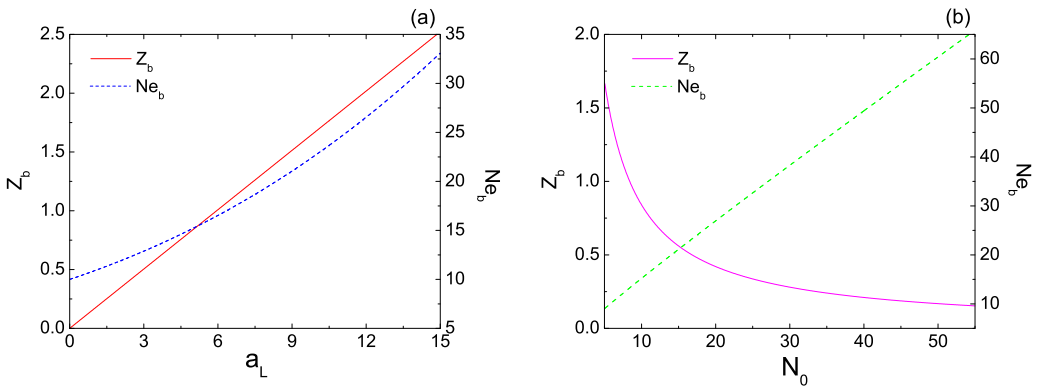

FIG. 1. (Color online) (a) The position of the density jump z_b and the peak of electron density Ne_b as a function of the incident laser amplitude for $N_0 = 10$, $\theta = 45°$. (b) z_b, Ne_b versus the initial plasma density with $a_L = 5$, $\theta = 45°$.

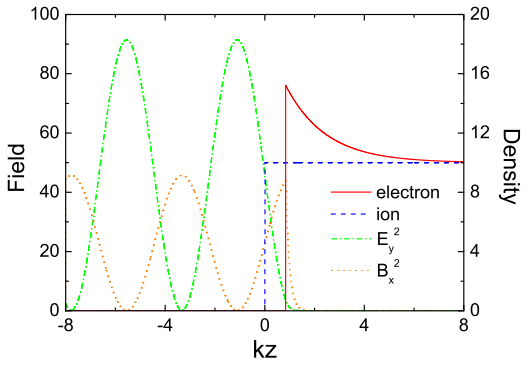

FIG. 2. (Color online) The spatial distribution of electron density (red solid line), ion density (blue dashed line), magnetic field (orange dotted line), and electric field (green dashed-dotted line), for s-polarized laser with $a_L = 5$, $N_0 = 10$, $\nu = 0.5$, $\theta = 45^\circ$.

N_0. Figure 1(a) shows z_b and Ne_b as functions of the incident laser amplitude for $N_0 = 10$, $\theta = 45^\circ$. As expected, with larger a_L the laser can push electrons deeper into the plasma. However, for the given laser and plasma parameters, the depth of the compressed electron layer remains around one tenth of the laser wavelength [27]. As a result, the electron density at the density jump Ne_b increases rapidly with the laser strength and can become several times the original target density. The influence of the initial plasma density on z_b and Ne_b are exhibited in Fig. 1(b) with $a_L = 5$, $\theta = 45^\circ$. It shows that for the given laser strength, the position of the effective vacuum-plasma interface z_b reduces noticeably with the increase of initial plasma density. While the electron density at the density jump Ne_b exhibits linear dependence on the initial plasma density. Physically, this is due to the fact that, for a larger original plasma density, the displacement of the electron plasma boundary will be less pronounced because the electrostatic field can easily balance the radiation pressure. This further improves the fact that the compression effect will weaken with the increase of initial plasma density.

III. COMPRESSION AND OSCILLATING EFFECTS ON S-POLARIZED LIGHT ABSORPTION

In the interaction of an ultraintense s-polarized laser pulse with a solid target, the ponderomotive forces, the zero-frequency component, as well as the 2ω oscillatory components both play important roles. The former determines the density profiles of the electrons and the latter drives the electron plasma surface oscillation at the second harmonics [28]. Besides, the absorption coefficient can be defined by using surface properties of the plasma, in particular the surface dielectric constant. In this way we can provide a modulation of the electron density compression effect on the laser absorption. Both of these will be discussed in more detail below.

A. The oscillation of the electron plasma surface driven by the 2ω ponderomotive force

In the following it is important to emphasize that we are considering the surface of overdense plasma where a major part of the incident light is reflected. Inside the plasma, the electromagnetic fields decay rapidly, and the thickness of skin layer l_s is much smaller than the wavelength of the laser. Based on the electron density profile derived from Sec. II, the distributions of the electromagnetic fields can be solved from the Helmholtz equation for the electric field:

$$\partial_z^2 E_y + (\varepsilon - \sin^2\theta) E_y = 0, \tag{11}$$

where ε denotes the dielectric function in the plasma. A typical solution is plotted in Fig. 2 with $a_L = 5$, $N_0 = 10$, $\theta = 45^\circ$, $\nu = 0.5$ (ν denotes the normalized electron-ion collision frequency). For $z < z_b$, it represents a standing wave, formed by the superposition of the incident laser wave with the reflected wave. However, beyond the density jump $z \geqslant z_b$, electrons are piled up deeply in a narrow region by the light pressure. Both the electric and magnetic fields evanesce quickly in the plasma, which are therefore sharply localized at the surface. Note the discontinuity in the magnetic field gradient at the density jump: This arises because the magnetic field changes its sign at the density jump.

As mentioned above, the electron distribution has a sharp surface located at the position z_b. It represents an effective surface from which the light is reflected. The ion density remains fixed with a sharp surface at $z = 0$. We assume that the skin layer with a thickness of l_s moves as a whole with the surface. Then for the s-polarized laser, the surface is driven harmonically by the ponderomotive force:

$$f_b(t) = -m_e c^2 \nabla \gamma_b(t), \tag{12}$$

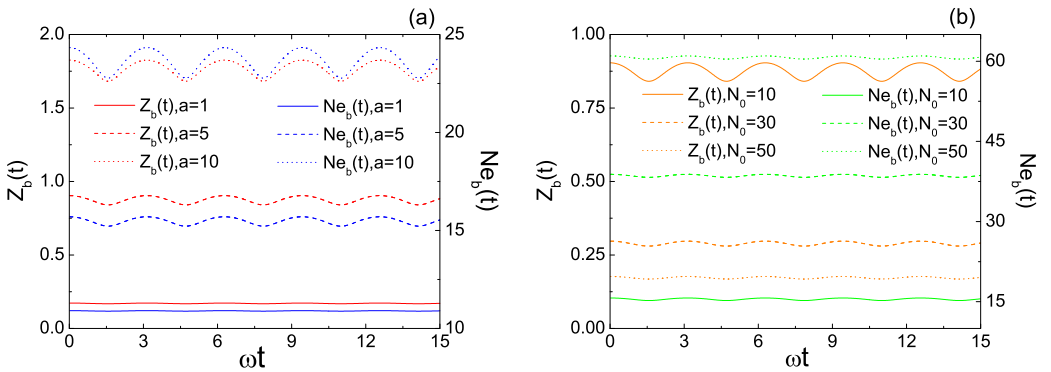

FIG. 3. (Color online) Temporal variation of the density jump z_b and the peak of electron density Ne_b for the s-polarized laser, with (a) $N_0 = 10$, $\nu = 0.5$, $\theta = 45^\circ$, and $a_L = 1, 5, 10$. (b) $a_L = 5$, $\nu = 0.5$, $\theta = 45^\circ$, and $N_0 = 10, 30, 50$.

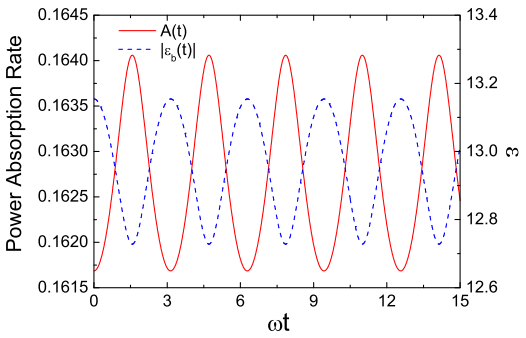

FIG. 4. (Color online) Temporal variation of the laser energy absorption rate $A(t)$ and the dielectric constant at the density jump $\varepsilon_b(t)$ for the s-polarized laser, with $a_L = 5$, $N_0 = 10$, $\nu = 0.5$, and $\theta = 45^\circ$.

where $\gamma_b(t) = \sqrt{1 + a_{Lb}^2(t)/2}$, $a_{Lb}(t) = eE_{yb}(t)/m_e\omega c$, and $E_{yb}(t)$ is the transverse electric field of the laser light at the surface. As we are mainly interested in highly overdense plasmas, i.e., $n_e/n_c \gg 1$, and omitting constant phase factors, $E_{yb}(t)$ can be approximated by [29]

$$E_{yb}(t) \approx 2E_L\sqrt{n_c/Ne_b}\cos(\omega t)\cos\theta. \tag{13}$$

Here E_L is the electric filed of the incident laser, and Ne_b means the compressed electron density at the surface as demonstrated above. Under the modulation of the 2ω-frequency ponderomotive force, the position of the electron plasma boundary will oscillate as

$$z_{b_{\rm osc}}(t) = z_b + \frac{\lambda}{4\pi^2}\sqrt{\frac{Ne_b n_c}{N_0^2}}\frac{a_{Lb}^2(t)}{2\gamma_b(t)}, \tag{14}$$

here z_b is the initial equilibrium position in Eq. (9), where the electrostatic fields balances the zero-frequency ponderomotive force. Owing to the conservation of the total electric charge, the peak value of the compressed electron density will also oscillate:

$$Ne_b(t) = N_0 + \frac{\alpha^2(t)N_0^2}{2n_c} + \frac{\alpha(t)N_0}{\sqrt{n_c}}\sqrt{N_0 + \frac{\alpha^2(t)N_0^2}{4n_c}}, \tag{15}$$

where $\alpha(t) = z_{b_{\rm osc}}(t)/\lambda$. The typical trajectory of $z_{b_{\rm osc}}(t)$ and the temporal variation of $Ne_b(t)$ are shown in Fig. 3.

Figure 3(a) presents the influence of the incident laser amplitude on the oscillation of the electron plasma surface. The laser strength a_L is varied from 1 to 10, while the initial plasma density keeps constant as $N_0 = 10$ with $\theta = 45^\circ$, $\nu = 0.5$. As expected, $z_{b_{\rm osc}}(t)$ and $Ne_b(t)$ both oscillate at 2ω frequency, yet also exhibit obvious perturbations which depend on the laser amplitude. With the increase of the laser strength, the amplitude of the electron plasma surface oscillation enlarges significantly, and the electron density can be compressed to a very high level. Figure 3(b) shows the time evolution of the $z_{b_{\rm osc}}(t)$ and $Ne_b(t)$ with different initial plasma densities for fixed $a_L = 5$ with $\theta = 45^\circ$, $\nu = 0.5$. We can see that the oscillation of the electron plasma surface decreases with the initial plasma density clearly. However, the change in the amplitude of $Ne_b(t)$ is not noticeable, only the average of the compressed electron density increases linearly with the initial plasma density as presented in Fig. 1(b).

B. The compression effect on s-polarized light absorption

The present investigation is restricted to one-dimensional geometry and considers a plane plasma layer with a sharp surface. The effect of the electron-ion collisions under these conditions will make the plasma behave like a metal surface with a finite conductivity. For the case of the oblique incidence of an s-polarized laser beam at an angle θ, the solution to Maxwell's equations results in the Fresnel formula for the reflectivity [30]:

$$R_s = \left|\frac{\sin(\theta - \theta_t)}{\sin(\theta + \theta_t)}\right|^2, \tag{16}$$

where $\theta_t = \arcsin[\sin\theta/n_b]$ is the generalized, complex angle of the transmitted light rays (from Snell's law), and $n_b = \sqrt{\varepsilon_b}$ means the local refractive index. Due to the oscillation of the compressed electron density, the dielectric constant at the surface ε_b will also vibrate with time in the form according to the Drude model [30]:

$$\varepsilon_b(t) = 1 - \frac{Ne_b(t)}{1 + i\nu}, \tag{17}$$

where $\nu = \nu_{ei}/\omega$, and ν_{ei} is the electron-ion collision frequency. Following the general theory of the metal optics, one

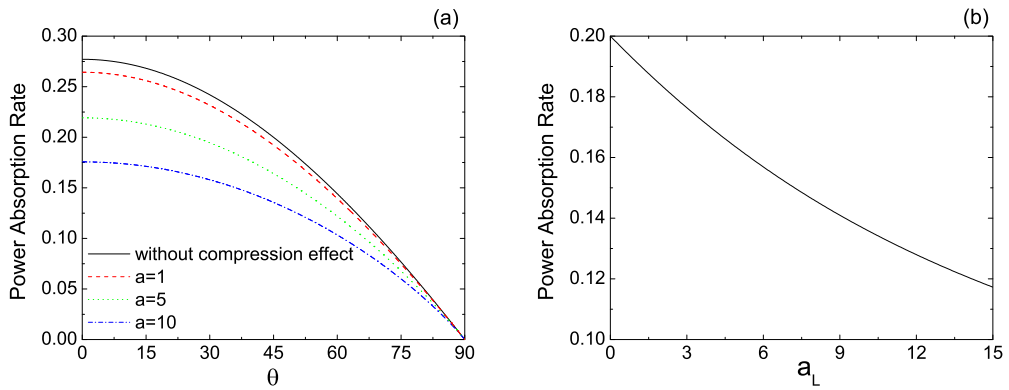

FIG. 5. (Color online) Angular dependence of s-polarized light absorption for $N_0 = 10$, $\nu = 0.5$, and $a_L = 1$, 5, 10. (b) The laser energy absorption rate as a function of the normalized laser amplitude for $N_0 = 10$, $\nu = 0.5$, $\theta = 45^\circ$.

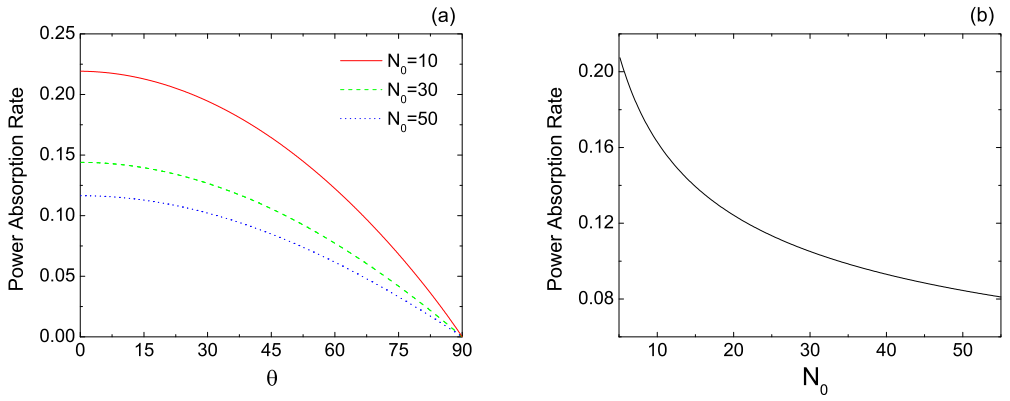

FIG. 6. (Color online) Angular dependence of s-polarized light absorption for $a_L = 5$, $\nu = 0.5$, and $N_0 = 10, 30, 50$. (b) The laser energy absorption rate as a function of the initial plasma density for $a_L = 5$, $\nu = 0.5$, $\theta = 45^\circ$.

can immediately write the laser absorption rate as

$$A_s(t) = 1 - R_s(t), \tag{18}$$

which also changes periodically with time. The temporal variation of the laser energy absorption rate $A_s(t)$ and the dielectric constant at the density jump $\varepsilon_b(t)$ are shown in Fig. 4. The red solid line represents $A_s(t)$, and the blue dashed line denotes $\varepsilon_b(t)$ according to Eq. (17). Both curves present 2ω oscillations, which is similar to the behavior of the electron plasma surface. The energy absorption rate oscillates between 0.16171 and 0.16408, which means that the amplitude of the oscillation is only 1.5% of the average. This proves that for the s-polarized laser plasma interaction, the influence of the electron plasma surface oscillation on the laser energy absorption is negligible. In order to quantitatively investigate the compression effect on the energy absorption, we apply the time-averaged $A_s(t)$ to describe the laser energy absorbed per unit time per unit volume in plasma:

$$A_s = \langle A_s(t) \rangle = \frac{1}{T} \int_0^T A_s(t) dt, \tag{19}$$

where T is the laser period.

It is of interest to consider the dependence of the laser energy absorption on the laser strength. As the comparison in Fig. 5(a) shows, the influence of the compression effect on laser absorption is particularly evident. With the increase of the laser intensity, the energy absorption rate decreases significantly due to the strengthening of the compression effect. Figure 5(b) presents the absorption rate as a function of the normalized laser amplitude for the fixed incident angle $\theta = 45^\circ$ with $N_0 = 10$, $\nu = 0.5$, which shows the absorption rate falling off in a more quantitative way. This can be interpreted by the compression of the electron density profile and the rapid evanescing of the electromagnetic fields in the plasma for such a sharp density gradient. In fact, while the electron density of the target front surface is compressed significantly by the strong laser pressure, only the electrons in the skin layer contribute to the absorption, the laser light can hardly penetrate into the plasma, and most of it will be reflected into the vacuum.

A further important issue is the influence of the initial plasma density on the laser energy absorption. Figure 6(a) shows the angular dependence of s-polarized light absorption for different initial plasma densities $N_0 = 10$, 30, and 50. In general, the absorption decreases monotonically with the angle of incidence, which is one of the characteristics of s-polarized light absorption. One observes that the absorption at each initial plasma density peaks at $\theta = 0^\circ$ because of the maximum penetration of the wave when the irradiation is normal to the target plane. For $N_0 = 10$, the lower density implies

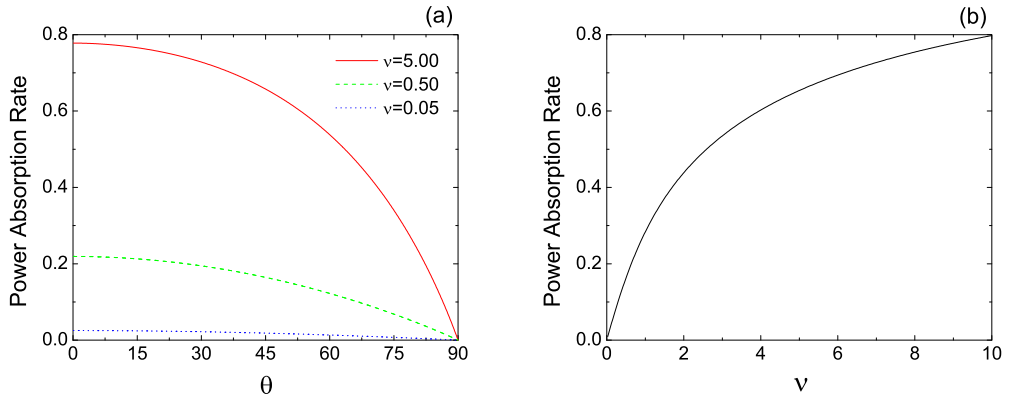

FIG. 7. (Color online) Angular dependence of s-polarized light absorption for $a_L = 5$, $N_0 = 10$, and $\nu = 0.05, 0.5, 5$. (b) The laser energy absorption rate as a function of the electron-ion collision frequency for $a_L = 5$, $N_0 = 10$, $\theta = 45^\circ$.

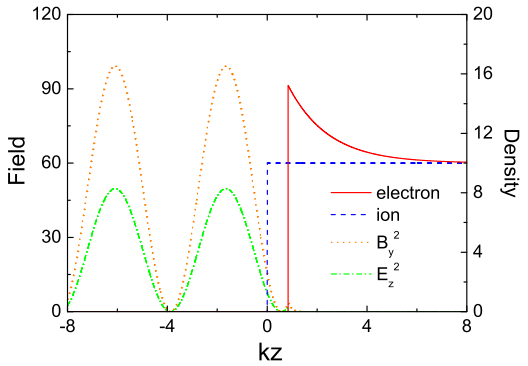

FIG. 8. (Color online) The spatial distribution of electron density (red solid line), ion density (blue dashed line), magnetic field (orange dotted line), and electric field (green dashed-dotted line), for p-polarized laser with $a_L = 5$, $N_0 = 10$, $\nu = 0.5$, $\theta = 45^\circ$.

smaller restoring forces and therefore larger amplitudes of the electron surface oscillations. Apparently, with the increase of N_0, the compression effect weakens, but the average electron density rises. As a result, the absorption rate falls off rapidly with the initial plasma density as illustrated in Fig. 6(b).

For s polarization, the collisionality is a vital parameter, since the inverse bremsstrahlung absorption also plays an important role in the absorption [31]. Figure 7(a) shows the angular dependence of s-polarized light absorption for three different electron-ion collision frequencies $\nu = 0.05$, 0.5, and 5. It is seen that for the low-collisionality case ($\nu = 0.05$), the energy absorption is almost not noticeable compared to the solid-collisionality case ($\nu = 5$). With the increase of the collisionality, the overall absorption rises obviously. However, this trend turns to slow down as depicted in Fig. 7(b) over a much wider range of collisionalities. It should be noticed that in our model, for simplicity, the collision frequency is assumed to be a constant at the density jump. In fact, the collisionality will decrease linearly with the electron density decay into the target [32]. Ignoring the dependence of collisionality upon the electron density may slightly overestimate the absorption in our model. While this overstatement is negligible (less than 10%) since the depth of the compressed electron layer remains around only one tenth of the laser wavelength, and the laser pulse can be thoroughly reflected within this region.

IV. COMPRESSION AND OSCILLATING EFFECTS ON *P*-POLARIZED LIGHT ABSORPTION

In the case of a p-polarized, obliquely incident laser pulse, the electron plasma surface is then mostly driven by the dominant longitudinal component of the laser **E** field. Electrons are thus pulled into the vacuum, where they are accelerated by the electromagnetic standing wave resulting from the incident and reflected laser waves, and subsequently pushed back into the target. In this regime we will see significant differences in the electron plasma surface oscillation and the laser energy absorption from the s polarization.

A. The oscillation of the electron plasma surface driven by the ω longitudinal electric field

For p light (electric vector in the plane of incidence), it is convenient to write the Helmholtz equation in terms of **B**, the complex magnetic field, in order to avoid the coupling between electromagnetic and electrostatic modes set up by the nonzero divergence of the laser electric field:

$$\partial_z^2 B_y - \varepsilon^{-1}\partial_z\varepsilon\partial_z B_y + (\varepsilon - \sin^2\theta)B_y = 0. \tag{20}$$

Here ε is the dielectric function in the plasma, and θ is the angle of incidence. The boundary conditions for Eq. (20) are freely outgoing waves at the vacuum side and evanescent waves at the high-density side. Therefore, by assuming electron density profile as supposed in Sec. II, Eq. (20) can be solved numerically (see Fig. 8). In the depletion region ($z < z_b$), since the electrons have been totally pushed out, the fields present standing-wave behavior like in the vacuum. While in the compression layer where $z \geqslant z_b$, the incident laser penetrates a skin depth into the dense plasma, and the electromagnetic fields decay significantly due to the high electron density level compressed by the light pressure.

Let us consider the case of a highly overdense plasma ($n_e/n_c \gg 1$), and neglect the magnetic field of the wave. Based on the Brunel's capacitor approximation [13], the driving electric field has a simple harmonic form

$$E_{zb}(t) \approx 2E_L \cos(\omega t)\sin\theta. \tag{21}$$

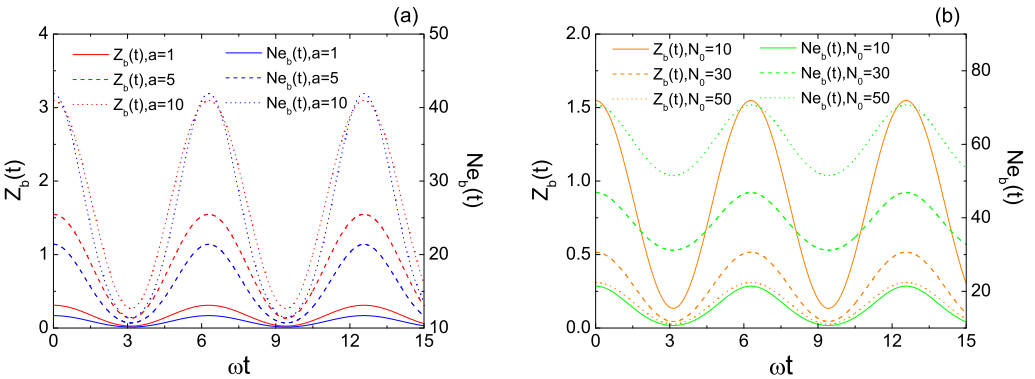

FIG. 9. (Color online) Temporal variation of the density jump z_b and the peak of electron density Ne_b for the p-polarized laser, with (a) $N_0 = 10$, $\nu = 0.5$, $\theta = 45^\circ$, and $a_L = 1$, 5, 10. (b) $a_L = 5$, $\nu = 0.5$, $\theta = 45^\circ$, and $N_0 = 10$, 30, 50.

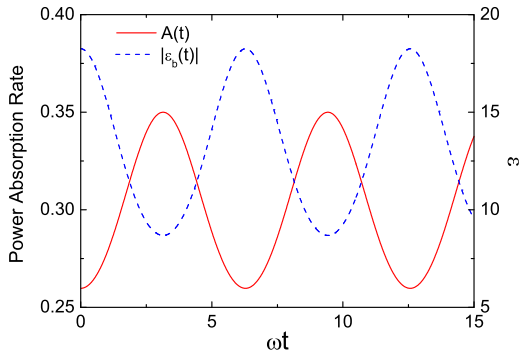

FIG. 10. (Color online) Temporal variation of the laser energy absorption rate $A(t)$ and the dielectric constant at the density jump $\varepsilon_b(t)$ for the p-polarized laser, with $a_L = 5$, $N_0 = 10$, $\nu = 0.5$, and $\theta = 45^\circ$.

Suppose this field pulls a sheet of electrons out from the initial equilibrium position z_b at a certain time t_0. Then, at $t_0 + \pi$, the driving field will reverse its direction, and push those electrons back into the target. As a consequence, the laser-plasma system behaves as a forced oscillator, and the electron-plasma surface response is synchronized with the driving electric field as

$$z_{b_{\rm osc}}(t) = z_b + \frac{\lambda}{\pi}\frac{n_c}{N_0} a_L \cos(\omega t)\sin\theta. \tag{22}$$

Due to the conservation of the total electric charge, the oscillation of the compressed electron density will obey the following equation:

$$Ne_b(t) = N_0 + \frac{\alpha^2(t)N_0^2}{2n_c} + \frac{\alpha(t)N_0}{\sqrt{n_c}}\sqrt{N_0 + \frac{\alpha^2(t)N_0^2}{4n_c}}, \tag{23}$$

where $\alpha(t) = z_{b_{\rm osc}}(t)/\lambda$. The time evolutions of $z_{b_{\rm osc}}(t)$ and $Ne_b(t)$ are displayed in Fig. 9 for different plasma and laser parameters. Figure 9(a) illustrates the influence of the laser intensity on the oscillation of the electron plasma surface. For a moderate intensity ($a_L = 1$), the displacement of the electron-plasma surface is much lower than the plasma skin depth, and the surface motion is also small. For higher intensities, the initial equilibrium position z_b will be pushed deeper into the plasma, and the surface oscillation becomes comparable to the plasma skin depth due to the increasing total force. To gain the dependence of the surface motion on the initial plasma density, we present $z_{b_{\rm osc}}(t)$ and $Ne_b(t)$ with different initial plasma densities for fixed $a_L = 5$ with $\theta = 45^\circ$, $\nu = 0.5$ in Fig. 9(b). Clearly, for the given laser amplitude, the decreasing of N_0 will strengthen the oscillation of the surface. Comparison between these three group curves also indicates that $z_{b_{\rm osc}}(t)$ turns out to be sensitive to N_0, whereas the oscillation amplitude of $Ne_b(t)$ almost remains constant (or grows slowly with N_0).

B. The compression effect on p-polarized light absorption

For the absorption of p-polarized laser energy, we employ the same method as in the s-polarized laser case to interpret the laser energy absorption in simple terms as reflected light from an oscillating mirror. An essential point is to account for the electron density compression effect on the energy absorption. The reflectivity is deduced from the Fresnel equations [30]:

$$R_p = \left|\frac{\tan(\theta - \theta_t)}{\tan(\theta + \theta_t)}\right|^2. \tag{24}$$

Subjected to the oscillating of $Ne_b(t)$ in Eq. (23), the dielectric constant at the surface ε_b will change periodically with time as in Eq. (17), and also the laser absorption rate:

$$A_p(t) = 1 - R_p(t). \tag{25}$$

The temporal variation of the laser energy absorption rate $A_p(t)$ and the dielectric constant at the density jump $\varepsilon_b(t)$ for the p-polarized laser are presented in Fig. 10. Compared to the results of the s polarization, both $A_p(t)$ and $\varepsilon_b(t)$ oscillate at ω frequency, mostly driven by the longitudinal component of the laser electric field. Moreover, the oscillation amplitude of $A_p(t)$ becomes considerably large, nearly 30% of the average, which is far beyond the value of the s polarization. Thus, the influences of the driving longitudinal laser electric field on the oscillation of the electron-plasma surface and laser energy absorption are much more significant for p polarization. Here and in the following, similar to the s polarization case, we will use the time-averaged $A_p(t)$ to describe the laser energy absorption for convenience:

$$A_p = \langle A_p(t)\rangle = \frac{1}{T}\int_0^T A_p(t)dt, \tag{26}$$

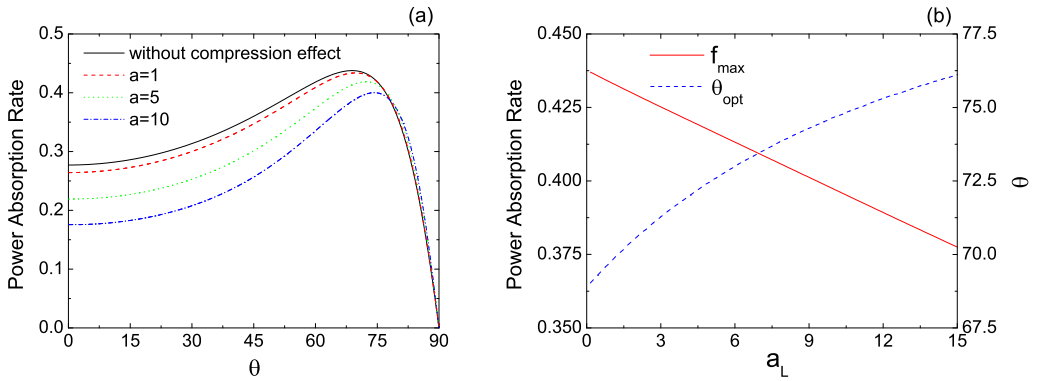

FIG. 11. (Color online) (a) Angular dependence of p-polarized light absorption for $N_0 = 10$, $\nu = 0.5$, and $a_L = 1, 5, 10$. (b) The maximum absorption rate $f_{\rm max}$ and the optimum angle $\theta_{\rm opt}$ as a function of the normalized laser amplitude for $N_0 = 10$, $\nu = 0.5$.

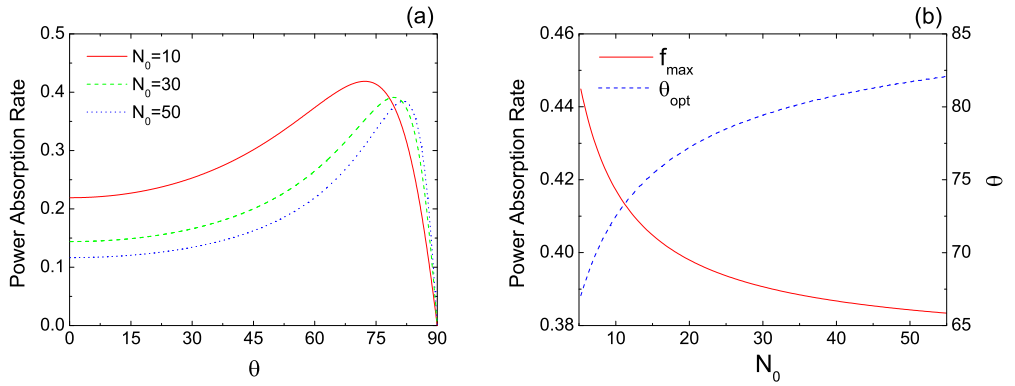

FIG. 12. (Color online) (a) Angular dependence of p-polarized light absorption for $a_L = 5$, $\nu = 0.5$, and $N_0 = 10, 30, 50$. (b) The maximum absorption rate $f_{\max}$ and the optimum angle θ_{opt} as a function of the initial plasma density for $a_L = 5$, $\nu = 0.5$.

where the brackets denote the average over one period of the laser field.

The influence of the laser strength on energy absorption is shown in Fig. 11(a). Without the compression effect, the absorption is considerably higher than that with the compression effect been considered. As the laser amplitude increases, the piled up electron wall can be compressed to a much higher level. Thus the incident laser will be reflected more thoroughly by the high-density electron wall, resulting in the drop of the absorption. To investigate this in a more quantitative way, we present the maximum absorption rate $f_{\max}$ and the optimum angle θ_{opt} as a function of the laser intensity in Fig. 11(b). Note the feature that the absorption peak decreases approximately linearly with laser intensity, and the increase in θ_{opt} reflects the shift of the angular absorption peak to higher angles. In addition, the absorption at normal incidence should be the same for both polarizations, and indeed it is the same, as one compares the result with the s polarization in Fig. 5(a) at $\theta = 0^\circ$. This behavior is consistent with that of Fresnel reflection from a sharp vacuum-plasma interface, which proves the efficiency of our model.

Figure 12(a) illustrates the angular dependence of the absorption for p-polarized light and initial plasma densities N_0 in the range 10–50 for $a_L = 5$, $\nu = 0.5$. Note that with the increase of N_0, the absorption peak moves to higher angles of incidence, narrows, and decreases. The narrowing in angle with increased initial density arises mainly because the wave spends progressively more of its time in the high-density plasma. The maximum absorption rate $f_{\max}$ and the optimum angle θ_{opt} as a function of the initial plasma density are plotted in Fig. 12(b). On the whole $f_{\max}$ reduces, while θ_{opt} increases with the initial plasma density, but these trends tend to slow down and get saturated as the density becomes high enough ($N_0 > 50$). This can be attributed to the weakening of the electron density compression effect with the increase of the initial plasma density for fixed laser intensity, as shown in Fig. 1(b). Moreover, the high-density plasma will reflect the incident light in a fashion similar to a metallic mirror, which leads to a higher reflectivity and poor coupling of the laser pulse to the plasma.

In order to complete the discussion of the p-polarized laser absorption, the angular dependence of the absorption on the electron-ion collision frequency is also considered, as displayed in Fig. 13(a), for three different collision frequencies. The peaks in the absorption curves correspond to the angular dependence of vacuum heating mechanism [13], where there is competition between the maximization of the electric field component along the density gradient and the wave penetration depth beyond the electron plasma surface. For $\nu = 0.05$, the condition is characteristic of a low-collisionality absorbing medium with the solid-state free-electron density. The overall absorption is small (<7%), and the maximum absorption occurs at $\theta \approx 80^\circ$. As ν increases, the absorption peak moves to smaller angle of incidence, and $f_{\max}$ increases, as shown in

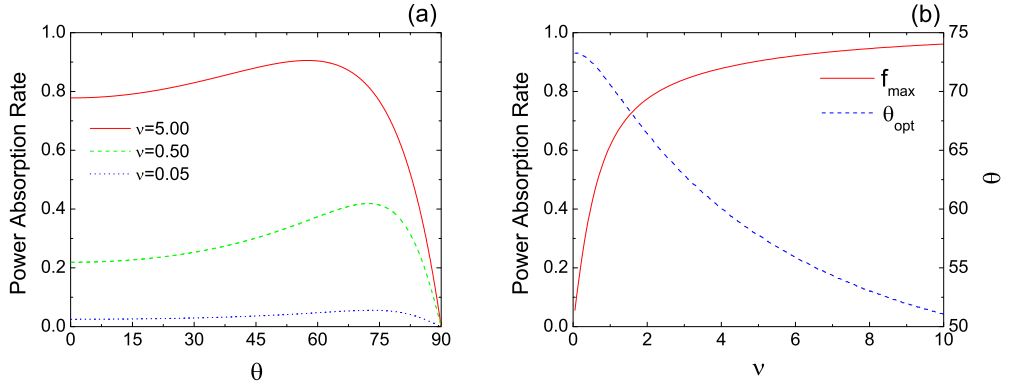

FIG. 13. (Color online) (a) Angular dependence of p-polarized light absorption for $a_L = 5$, $N_0 = 10$, and $\nu = 0.05$, 0.5, 5. (b) The maximum absorption rate $f_{\max}$ and the optimum angle θ_{opt} as a function of the electron-ion collision frequency for $a_L = 5$, $N_0 = 10$.

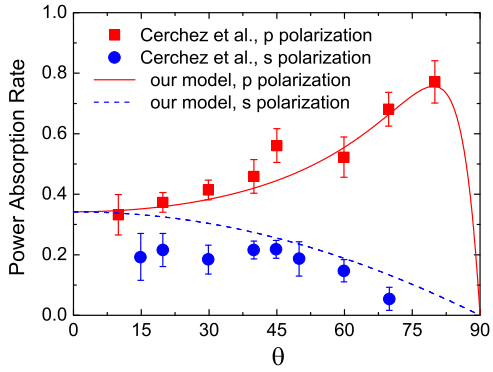

FIG. 14. (Color online) Theoretical angular dependence of the laser absorption (for $N_0 = 100$, $\nu = 3$), compared with the experimental data from [34] for 8 fs, 790 nm laser pulses irradiated an aluminum target at an average intensity of 5×10^{16} W/cm^2.

Fig. 13(b). For collisionality in the solid $\nu = 5$, the absorption are largely due to collisional or inverse bremsstrahlung absorption, and the resonance absorption is quenched since the electron density is far beyond the resonance condition [33].

V. COMPARISON WITH EXPERIMENT AND CONCLUSION

Comparison of our model calculation with the experimental results of Cerchez *et al.* [34] is displayed in Fig. 14, which shows good agreement with appropriate choice of the parameters. In the experiment, their laser pulse parameters ($\sim$8 fs and high-contrast $\sim10^8$) allowed us to study the absorption under novel conditions where the pulse energy is basically directly transferred to the solid matter. The energy of these ultrashort laser pulses can be efficiently absorbed up to $\approx$77% by a plasma at density close to solid state, characterized by a very steep profile. The absorption of the p-polarized laser pulses significantly exceeds the s-polarization absorption. Computer simulations are consistent with the experimental results for a plasma profile of $L/\lambda \approx 0.01$, which is just the extremely short scale length required in our assumption of sharp boundary. For the theoretical calculation, we consider a solid aluminum target with the ionization degree $Z = 3$, such that $n_e = 2\times10^{23}$ cm^{-3}. As the target is irradiated with 0.8 μm light from a Ti:sapphire laser, we have $n_e/n_c \approx 100$. Suppose that the plasma is heated to 170 eV after just 8 fs irradiation by the incident laser, so that according to [11]

$$\nu_{ei} = \frac{4(2\pi)^{1/2}}{3}\frac{n_e Z e^4}{m_e^2 v_{te}^3}\ln\Lambda \approx 2.91\times10^{-6} Z n_e T_e^{-3/2}\ln\Lambda s^{-1}, \quad (27)$$

where T_e is the electron temperature and $\ln\Lambda$ is the Coulomb logarithm, we have $\nu_{ei}/\omega = 3$ at the initial density. The resulting absorption curves calculated from Eqs. (16) and (24) are shown in Fig. 14 for the s-polarized and p-polarized laser, respectively. Obviously the two curves agree well with the experimental data, especially for the p polarization. Thus, our calculation clearly confirms the observations and the validation of our model should be evident. However, when the laser pulse is typically longer than 100 fs, or a prepulse is present, a preplasma will be formed in front of the target and undergoes hydrodynamic expansion. Then the assumption of sharp boundary becomes invalid and our model may fail. Besides, though our model is consistent with experimental data at low intensities, the electron density compression and oscillating effects predicted by our model at ultraintense intensities should be further examined by future experiments.

In conclusion, we present an analytical model for ultrashort ultraintense laser absorption. This model is based on the assumption of a sharp boundary, which requires an extremely short scale length, and the details of the electron dynamics are neglected. In contrast to previous theoretical papers, the analysis undertaken in the present paper sheds light on the electron density compression and oscillating effects on the laser energy absorption. The general scaling law of the electron density compression effect depending on laser intensity and initial plasma density is derived, and the temporal variation of the laser absorption due to the boundary oscillating effect is presented. The theory should provide quantitative guidance for applications involving high-order laser harmonics and particle sources.

ACKNOWLEDGMENTS

This work was supported by the National Natural Science Foundation of China (Grants No. 11175253, No. 91230205, No. 11174303, No. 11204329, No. 11205243, No. 11127901, No. 11275269, and No. 11305264), the National High-Tech 863 Project, the Research Project of NUDT, and the National Basic Research Program of China (Grants No. 2013CBA01504 and No. 2011CB808100).

[1] M. M. Murnane, H. C. Kapteyn, M. D. Rosen, and R. W. Falcone, Science **251**, 531 (1991).
[2] T. P. Yu, A. Pukhov, Z. M. Sheng, F. Liu, and G. Shvets, Phys. Rev. Lett. **110**, 045001 (2013).
[3] A. L'Huillier, K. L. Schafer, and K. C. Kulander, J. Phys. B **24**, 3315 (1991).
[4] A. Modena, Z. Najmudin, A. E. Dangor, C. E. Clayton, K. A. Marsh, C. Joshi, V. Malka, C. B. Darrow, C. Danson, D. Neely, and F. N. Walsh, Nature (London) **377**, 606 (1995).
[5] H. B. Zhuo, Z. L. Chen, W. Yu, Z. M. Sheng, M. Y. Yu, Z. Jin, and R. Kodama, Phys. Rev. Lett. **105**, 065003 (2010).
[6] T. P. Yu, A. Pukhov, G. Shvets, and M. Chen, Phys. Rev. Lett. **105**, 065002 (2010).
[7] Z. Y. Ge, Y. Yin, S. X. Li, M. Y. Yu, T. P. Yu, H. Xu, H. B. Zhuo, Y. Y. Ma, F. Q. Shao, and C. L. Tian, New J. Phys. **14**, 103015 (2012).
[8] F. N. Beg, A. R. Bell, A. E. Dangor, C. N. Danson, A. P. Fews, M. E. Glinsky, B. A. Hammel, P. Lee, P. A. Norreys, and M. Tatarakis, Phys. Plasmas **4**, 447 (1997).

[9] T. Tanimoto *et al*., Phys. Plasmas **16**, 062703 (2009).
[10] D. F. Price, R. M. More, R. S. Walling, G. Guethlein, R. L. Shepherd, R. E. Stewart, and W. E. White, Phys. Rev. Lett. **75**, 252 (1995).
[11] W. L. Kruer, *The Physics of Laser Plasma Interactions* (Addison-Wesley, New York, 1988).
[12] W. L. Kruer and K. Estabrook, Phys. Fluids **28**, 430 (1985).
[13] F. Brunel, Phys. Rev. Lett. **59**, 52 (1987).
[14] P. Gibbon and A. R. Bell, Phys. Rev. Lett. **68**, 1535 (1992).
[15] P. Gibbon, Phys. Rev. Lett. **73**, 664 (1994).
[16] M. G. Haines, M. S. Wei, F. N. Beg, and R. B. Stephens, Phys. Rev. Lett. **102**, 045008 (2009).
[17] P. Gibbon, A. A. Andreev, and K. Yu. Platonov, Plasma Phys. Control. Fusion **54**, 045001 (2012).
[18] B. Dromey, S. Kar, M. Zepf, and P. Foster, Rev. Sci. Instrum. **75**, 645 (2004).
[19] F. Tavella, A. Marcinkevicius, and F. Krausz, Opt. Express **14**, 12822 (2006).
[20] W. Yu, Z. M. Sheng, M. Y. Yu, J. Zhang, Z. M. Jiang, and Z. Xu, Phys. Rev. E **59**, 3583 (1999).
[21] J. Sanz, A. Debayle, and K. Mima, Phys. Rev. E **85**, 046411 (2012).
[22] H. B. Cai, W. Yu, S. P. Zhu, and C. T. Zhou, Phys. Rev. E **76**, 036403 (2007).
[23] Z. Y. Ge *et al*., Phys. Plasmas **20**, 073301 (2013).
[24] D. Bauer and P. Mulser, Phys. Plasmas **14**, 023301 (2007).
[25] A. Macchi, F. Cattani, T. V. Liseykina, and F. Cornolti, Phys. Rev. Lett. **94**, 165003 (2005).
[26] J. Meyer-ter-Vehn, A. Pukhov, and Z. M. Sheng, *Atoms, Solids, and Plasmas in Super-Intense Laser Fields*, edited by D. Batani *et al*. (Kluwer Academic/Plenum, Dordrecht, 2001).
[27] S. X. Luan, W. Yu, M. Y. Yu, G. J. Ma, Q. J. Zhang, and Z. M. Sheng, Phys. Plasmas **18**, 042701 (2011).
[28] W. Yu, M. Y. Yu, Z. M. Sheng, and J. Zhang, Phys. Rev. E **58**, 2456 (1998).
[29] R. Lichters, J. Meyer-ter-Vehn, and A. Pukhov, Phys. Plasmas **3**, 3425 (1996).
[30] M. Born and E. Wolf, *Principles of Optics* (Pergamon, New York, 1980).
[31] P. J. Catto and R. M. More, Phys. Fluids **20**, 704 (1977).
[32] I. P. Shkarofsky, T. W. Johnston, and M. O. Bachynski, *The Particle Kinetics of Plasmas* (Addison-Wesley, Reading, MA, 1966).
[33] H. M. Milchberg and R. R. Freeman, J. Opt. Soc. Am. B **6**, 1351 (1989).
[34] M. Cerchez, R. Jung, J. Osterholz, T. Toncian, O. Willi, P. Mulser, and H. Ruhl, Phys. Rev. Lett. **100**, 245001 (2008).